

Ferroelectric ordering in lamellar CuInP_2S_6

V. Maisonneuve and V. B. Cajipe*

Institut des Matériaux de Nantes, CNRS UMR 6502, 2, rue de la Houssinière, B.P. 32229, 44322 Nantes Cedex 3, France

A. Simon, R. Von Der Muhll, and J. Ravez

Institut de Chimie de la Matière Condensée de Bordeaux, Château Brivazac, Avenue du Dr. A. Schweitzer, F-33600 Pessac, France

(Received 18 May 1997)

The lamellar compound CuInP_2S_6 is presented as an unusual example of a collinear, two-sublattice ferroelectric system. Single-crystal x-ray diffraction is used to study the thermal evolution of the polar character of its structure. The results are consistent with the occurrence of a first-order, order-disorder transition at $T_c = 315$ K and provide indirect evidence for copper hopping motions. Estimates for the spontaneous polarization are calculated at various temperatures from the atomic coordinates and found to agree well with dielectric measurements. The example of CuInP_2S_6 suggests that cooperative dipole behavior may generally arise when d^{10} cations (e.g., Cu^I and In^{III}) susceptible to second-order Jahn-Teller distortions are embedded in a matrix of restricted dimensionality. [S0163-1829(97)01238-1]

I. INTRODUCTION

The occurrence of a ferroelectric phase is premised on the possibility of stabilizing atoms in off-center sites within a crystal at some temperature. Although over two hundred compounds exhibiting a reversible macroscopic polarization have been identified and numerous experimental techniques employed to investigate their attendant critical phenomena,¹ the microscopic origin of this behavior remains unclear in most cases. Indeed, only in this decade have first-principles calculations been applied to model the phase transitions observed in BaTiO_3 , the oldest of the well-studied ferroelectric perovskite oxides.^{2,3} Odd-parity configurations are easily envisioned in terms of low-energy motions perturbing the ideal cubic perovskite structure. However, the essential role of hybridization between the Ti $3d$ and O $2p$ states in weakening the short-range repulsions that inhibit long-range polar order became apparent only after detailed calculations of the electronic density of states³ in BaTiO_3 and PbTiO_3 . It thus seemed worthwhile considering other systems in which ferroelectricity might be more intuitively recognized as being electronically driven.

Recently, we reported ordered dipole arrangements in the layered materials $\text{Cu}^I\text{M}^{III}\text{P}_2\text{S}_6$ ($M = \text{Cr}, \text{In}$).^{4,5} These thiophosphates consist of lamellae defined by a sulfur framework in which the metal cations and P-P pairs fill the octahedral voids; within a layer, the Cu, M, and P-P form triangular patterns (Fig. 1, top left). The prospect of long-range dipole order appearing within such a lattice was raised by the observation of a smeared electronic density associated with the Cu^I ion in the paraelectric CuCrP_2S_6 phase ($T > 190$ K) (Refs. 6 and 7) as well as in the room-temperature (RT) structure of the related compound CuVP_2S_6 .⁸ This density extends along the normal to the layer and may be accounted for crystallographically by using three types of partially filled sites with large thermal factors: an off-center and quasitrigonal Cu^I , an almost central or octahedral Cu^2 , and a third nearly tetrahedral Cu^3 in the interlayer space (Fig. 1, top right). A twofold axis through the octahedral center and

in the plane of the layer doubles the number of positions per CuS_6 unit, the quasitrigonal Cu^I being predominantly occupied in both CuCrP_2S_6 and CuVP_2S_6 at RT (monoclinic space groups $C2/c$ and $C2$, respectively).^{6,8} Such a distribution may be interpreted in terms of a static, positional disorder. However, the existence of a stable, octahedrally coordinated Cu^I is doubtful from a stereochemical viewpoint:⁹ monovalent copper has a preference for low coordination that is attributable to a second-order Jahn-Teller coupling between the filled $3d^{10}$ manifold and empty $4s$ orbital.¹⁰⁻¹²

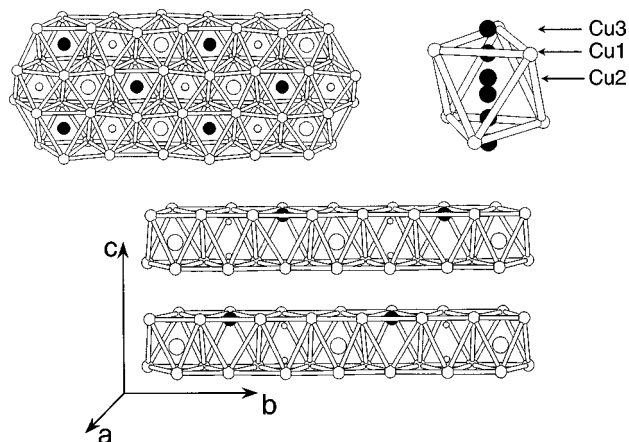


FIG. 1. Top left: Projection onto the a - b plane of the CuInP_2S_6 structure showing the triangular sublattices formed by the copper and indium cations and the P-P pairs. Top right: A sulfur octahedral cage showing the various types of copper sites: the off-center Cu^I , the almost central Cu^2 , and Cu^3 in the interlayer space. At $T > 315$, a twofold axis through the center doubles the number of sites per CuS_6 ; two off-center sites become inequivalent when unequally occupied at $T < 315$ K. Bottom: Two layers of CuInP_2S_6 shown in the ferroelectric phase ($T < 315$ K). The up (down) shifted Cu^I (In^{III}) ions are represented by the larger black (white) circles in the octahedra; the smaller white circles are the P. The monoclinic lattice parameters at room temperature are $a = 6.0956(4)$ Å, $b = 10.5645$ Å, $c = 13.6230(9)$ Å, and $\beta = 107.101(3)^\circ$.

$\text{Cu}2$ should therefore not be considered an equilibrium site. A more likely cause of the density smearing would be the occurrence of large-amplitude, thermal hopping motions of the Cu^I ions between potential wells flanking the central site, and into the adjacent interlayer site at higher temperatures. Electronic density around the octahedral center would then indicate a nonzero probability of finding the copper ion between two equivalent $\text{Cu}1$ positions. Granting that occupation of an off-center site produces a local electric dipole moment, it may be said that at high enough temperatures a given CuMP_2S_6 contains Cu^I dipoles that randomly flip between an up and down state, yielding a macroscopically non-polar configuration. Ordering may then be conceived in terms of a cooperative freezing of these motions, with a breaking of the twofold symmetry and dipole correlations possibly locking in a net polarization.

In CuVP_2S_6 no such transition has been detected down to 20 K.¹³ On the other hand, CuCrP_2S_6 exhibits an ordered phase at $T \leq 150$ K in which every layer contains alternating rows of up- and down-shifted Cu^I (space group Pc), i.e., a dipole arrangement with a null net polarization.⁴ A polar copper sublattice was observed in the third isomorph CuInP_2S_6 : at RT, 90% of the Cu^I ions in this compound occupy a site ($\text{Cu}1''$) shifted upward by 1.58 Å from the midplane of the layer (noncentrosymmetric monoclinic space group Cc ; see Fig. 1, bottom).⁵ The In^{III} ions were likewise found to be shifted but downward by only ≈ 0.2 Å from the midplane, forming a second polar sublattice. Dipole ordering in CuMP_2S_6 thus appears to derive from a conjunction of two effects: an off-centering instability associated with a d^{10} electronic configuration ($3d^{10} \text{Cu}^I$ and $4d^{10} \text{In}^{\text{III}}$), and the cations being constrained by the layered morphology to undergo antiparallel displacements. The resultant arrangement in CuInP_2S_6 is that of an uncompensated, two-dimensional *ferrielectric*.¹⁴ Because the Cu^I off centering is much greater than that of In^{III} , a fairly large spontaneous polarization P_s may be expected to appear normal to the layers. Previous calorimetry and electric permittivity measurements on CuInP_2S_6 have indicated an anomaly at $T_C = 315(5)$ K consistent with the occurrence of a ferroelectric-paraelectric transition, i.e., P_s vanishing upon heating to this temperature.¹⁵

In this paper, we examine the thermal evolution of the unusual ferrielectric structure of CuInP_2S_6 using single-crystal x-ray diffraction. Cooling is found to enhance the polarity of the copper and indium sublattices in the ferroelectric phase, while warming above T_C leads to its loss as the Cu^I ions assume a twofold symmetric distribution over the various copper sites and the In^{III} ions move to central octahedral positions. Temperature-dependent electron and probability densities provide indirect evidence for copper hopping motions in both the paraelectric and ferroelectric phases. The spontaneous polarization \mathbf{P}_s was calculated from the atomic coordinates and site occupations as a function of temperature; concomitant strains in the structure were also monitored. These crystallographic results are discussed in relation with dielectric measurements as well as the probable nature of the phase transition in this material. Finally, we suggest that cooperative dipole effects similar to those observed in CuInP_2S_6 may generally be created by embedding

d^{10} cations susceptible to second-order Jahn-Teller distortions in a matrix of restricted dimensionality.

II. EXPERIMENTAL TECHNIQUES AND DATA ANALYSIS

Crystals of CuInP_2S_6 were prepared by solid state reaction as previously described.⁵ The temperature-dependent x-ray-diffraction studies were carried out on the $0.09 \times 0.09 \times 0.02$ mm³ crystal used for the RT structural determination. Auxiliary physical measurements (see below) were made on samples approximately 10 mm² in area and 16 μm thick.

Single-crystal x-ray-diffraction data were collected using either an Enraf-Nonius CAD4-Kappa or a Siemens 4-circle diffractometer, each outfitted with a Mo $K-L_{2,3}$ x-ray tube and a graphite monochromator ($\lambda = 0.71073$ Å). The former was equipped with a heated N_2 gas blower regulated by a commercial temperature controller for the $T > 298$ K measurements. The latter had a Siemens LT-2A low temperature device mounted on the χ circle with a nozzle directing a stream of cold N_2 gas over the crystal; the power delivered to heaters in the nozzle and LN_2 reservoir was adjusted by a closed-loop circuit to control the temperature in the $T < 298$ K experiments. In both cases, the thermocouples were located a few millimeters upstream of the crystal. To evaluate the thermal gradient along the stream and obtain the correct crystal temperature, prior temperature measurements were made at different set points with a thermocouple fixed at the sample position. The temperature thus measured had an estimated uncertainty of and stability better than ± 1 K. Data were collected at seven temperatures ($T = 153, 243, 298, 305, 318, 353, \text{ and } 393$ K). For $T \leq 353$ K, reflection intensities from half of the reciprocal space ($k \geq 0$) were recorded while omitting those systematically absent due to the C centering. The $T = 243$ K data set, for example, contained 4822 reflections; equivalent reflections were averaged after Lorentz-polarization and absorption corrections to yield a set of 2179 independent hkl 's with $I > 3\sigma(I)$. In the $T = 318$ and 353 K data sets, Friedel pairs were averaged following indications of centrosymmetry given by preliminary analysis of the first $T > T_C$ set. Data from a quarter of the reciprocal space were recorded at $T = 393$ K. These $T > T_C$ data sets contained a smaller number of independent reflections [e.g., 829 with $I > 3\sigma(I)$ for $T = 318$ K]. Structural refinements were carried out using the MOLEN (Ref. 16) and PROMETHEUS (Ref. 17) suites of programs. The cell parameters used were those obtained in a previous variable temperature x-ray powder diffraction study.¹⁵ The recording and refinement conditions are summarized in the auxiliary material.¹⁸

As mentioned above, electronic densities spread over a relatively large volume may be modeled crystallographically by distributing the atom over several ‘split’ positions. Each position \mathbf{x}_i is assigned an occupancy c_i such that $\sum_i c_i = 1$. The occupancy conservation condition may be relaxed when a sum less than unity may be reasonably expected, e.g., in fast ionic conductors. Not all positions used are necessarily equilibrium sites. Generally, a more physical representation of the distribution is given by the probability of finding an atom within a volume element. For an isolated atom or site, this probability, formally called the one-particle probability

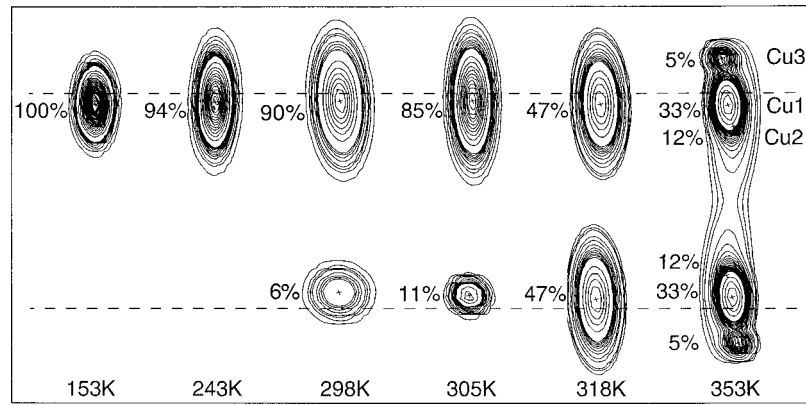


FIG. 2. Thermal evolution of the different copper site occupancies and the corresponding probability density contours in CuInP_2S_6 (see text and Fig. 1, top right). The crosses mark the refined positions, and the dashed lines indicate the upper and lower sulfur planes of a single layer. Occupancies not adding up to 100% indicate the presence of diffuse electronic densities between the off-center sites and/or in the interlayer space. The contours are given in \AA^{-3} , the values for the lowest and highest displayed temperatures being 153 K, 25–75 (50), 75–775 (100), and 775–27 775 (1000); and 353 K, 40–100 (30), 100–800 (100), and 800–5800 (1000), where the intervals are inscribed in parentheses.

density function, is obtained as the Fourier transform of the temperature factors.¹⁷ Note that because the so-called temperature factors may not exclusively be due to thermal vibrations but could also reflect the existence of static (space-averaged) or other dynamic (time-averaged) types of disorder, the alternative expression “atomic displacement parameter” (ADP) has recently appeared in the literature.¹⁹ Generally, the ADP is anisotropic and described by a symmetrical tensor \mathbf{U} with six independent components; the equivalent isotropic thermal factor is given by the expression $B_{\text{eq}} = 8\pi^2 (1/3\text{Tr}\mathbf{U})$. In the case of a distribution in which the amplitudes of thermal motion become comparable with the distances separating the sites, the intersite density cannot unambiguously be attributed to a particular position. The probability would then be more correctly represented by the weighted sum of the Fourier transforms of the ADP of all the contributing sites, i.e., a joint probability density function (JPDF).¹⁷

Smear electronic densities may also be described crystallographically via a nonharmonic model, i.e., by introducing terms of orders higher than two in the expansion for the ADP associated with a *fully* occupied site. This would be appropriate in cases where there is some ambiguity regarding the origin of the smearing, i.e., pronounced anharmonic motions (single local maximum in the probability density), or the presence of static or dynamic disorder involving weakly resolved positions (two or more density maxima). A Gram-Charlier type expansion has been shown to be most suitable for such an analysis.¹⁹ The PROMETHEUS package was used to discern possible nonharmonic effects within the CuInP_2S_6 structure as well as calculate the probability densities for the Cu^{I} and In^{III} ions.

To support the structural results, electrical characterization supplementing previously reported dielectric data¹⁴ were sought by measuring the ferroelectric hysteresis loop at RT and the pyroelectric coefficient at $T < 315$ K. The former was done using a Sawyer-Tower type circuit and the latter by a thermal depolarization method.

III. RESULTS

As in the earlier room-temperature structural study,⁵ the first stages of the refinement of the various data sets con-

sisted of finding the indium, sulfur, and phosphorous positions using Patterson, Fourier, and difference Fourier maps. The structural refinement for the $T < T_C$ ($= 315$ K) and initially for the 318-K data was carried out within the monoclinic space-group Cc . In each case, the overall features of the known layered framework and triangular indium sublattice were found to be conserved. A new difference Fourier map could then be calculated to locate the copper atom. The electron densities gave clear indications of the degree of polarity of the copper sublattice at the various temperatures. For $T < 315$ K, the densities were dominated by a maximum around the upper off-center site Cu1^{II} . At 318 K, density maxima of equal height were detected at the upper and lower off-center sites, implying the existence of a twofold axis through the center of the CuS_6 octahedral unit, parallel to the b axis. The structural models for $T > 315$ K were then refined within the nonpolar space group $C2/c$. In other words, it was assumed that the ferroelectric-paraelectric phase transition occurs with the space symmetry change Cc (point group m) to $C2/c$ (point group 2). The final stages of the structure refinement essentially determined how best to account for the copper electronic densities in terms of the occupancies of the different possible copper positions Cu1 , Cu2 , and Cu3 (Fig. 1, top right). The smaller off-center displacement for In^{III} was disclosed by comparing its z coordinate with that of the center of the S_6 octahedral cage through which the layer midplane passes (at $z = 0.25$ in the paraelectric phase). For the most part, the use of anisotropic harmonic ADP for all the atoms was found to be sufficient. The cell parameters, atomic positions, and ADP at various temperatures are given in the auxiliary material.¹⁸ Figure 2 displays the copper site occupancies and the corresponding probability density contours¹⁷ obtained as a function of temperature.

At 153 K, the Cu1^{II} position located 1.55 \AA above the layer midplane is 100% filled. Refining the occupancy did not lead to any significant deviation from unity. The copper sublattice may thus be said to be completely polar at this temperature, with the Cu^{I} undergoing harmonic vibrations within its off-center site.

Upon heating, the Cu1^{II} occupancy decreases to 94% and

90% at 243 and 298 K, respectively, and to 85% at 305 K just below the transition. Simultaneously, the Cu1^d site starts to fill. At 243 K, only a residual electronic density could be associated with this lower off-center site but its occupation could be refined at 298 and 305 K. The copper site occupancies do not add up to 100% at these temperatures. This is not surprising since electronic densities too weak and diffuse to be modeled by additional positions were detected in the intersite and interlayer regions. Such observations imply that hopping motions between the Cu1^u potential minimum and the probably shallower one at Cu1^d , as well as between an intra- and interlayer site, already occur in the ferroelectric phase. The existence of reversely polar domains may however not be excluded.

Above $T_C=315$ K, the Cu1^u and Cu1^d sites become equivalent (Cu1), i.e., the structure becomes centrosymmetric with the appearance of a twofold axis through the octahedral center. The site occupancies in this temperature regime are taken twice and summed to obtain the total distribution. Cu1 fills to slightly less than 50% at 318 K, the copper “deficit” here being associated with diffuse electronic densities indicative of thermal hopping. At 353 K, the Cu1 occupancy decreases to 33% and the Cu2 and Cu3 sites start to fill, presumably as more energy becomes available for the hopping motions. Cu2 , located an appreciable 1.20 Å from the octahedral center, was refined as being 12% occupied and having rather large ADP’s ($B_{\text{eq}} \approx 12 \text{ \AA}^2$). This leads to a very flat central region in the JPFD, which is consistent with the unlikelihood of a statically stable and octahedrally coordinated Cu^1 . The Cu3 site in the interlayer space is only 5% filled but appears as a distinguishable maximum in the JPFD. Overall, the copper probability density at 353 K is markedly anisotropic: its elongation perpendicular to the layer and the presence of maxima at the Cu1 and Cu3 positions are consistent with the occurrence of Cu1-Cu1 and Cu1-Cu3 type jumps. A three-copper-site model was likewise applied to data recorded at 393 K, with Cu1/Cu2/Cu3 occupancies of 43%/3%/3%, the Cu2 position being closer to the octahedral center and the Cu3 located more deeply in the interlayer space.¹⁸ These model parameters and the observation of residual electronic densities between layers are suggestive of increased Cu1-Cu3 -type hopping at this higher temperature. Cu^1 migration along the normal to the layers inferred from the above has been confirmed by ionic conductivity measurements on this compound in the paraelectric phase.²⁰

The polarity of the indium sublattice also evolves with temperature: the In^{III} downward displacement decreases from 0.24 Å at 153 K to 0.18 Å at 305 K and vanishes at $T > 315$ K. No residual electronic densities indicative of upshifted In^{III} , i.e., the presence of reversely polar domains were found after refinement of the $T < 315$ K data. On the other hand, residues of up to $\approx 2e^-/\text{\AA}^2$ were observed around the indium position in the difference Fourier maps obtained after the $T > 315$ K data refinements. This suggests that the off-centering instability for In^{III} is already present in the paraelectric phase. Analyses including fourth-order tensors in the In^{III} ADP’s were performed on the various $T > 315$ K data sets. Only that for the 393 K data provided an improvement over the purely harmonic model based on the flatness of the difference Fourier map and application of the

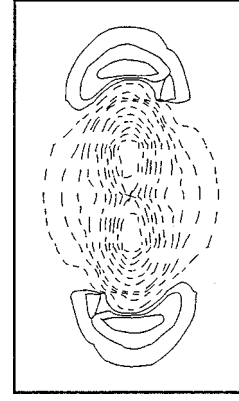


FIG. 3. The fourth-order deformation density map for In^{III} at 393 K which gives the difference between the probability densities obtained with a nonharmonic and harmonic expansion for the thermal factor. Note the positive (negative) densities in the $\approx 0.6 \text{ \AA}$ off-center (near-center) regions. Contours are drawn at -5210 and -660 \AA^{-3} , -660 to -60 \AA^{-3} every 200 (dashed lines), $26-176 \text{ \AA}^{-3}$ every 50 (solid lines).

Hamilton test.²¹ Small probability densities in the off-center regions were thus disclosed as shown in Fig. 3. Examination of the P_2S_6 group shows that it is not centrosymmetric either at $T < 315$ K. The P-P pair shifts below the layer midplane in the ferroelectric phase but by only 0.01 Å at $T = 305$ K and 0.03 Å at 153 K.

An estimate for the spontaneous polarization \mathbf{P}_s may be calculated from the atomic coordinates and site occupations at a given temperature using the simple expression

$$\mathbf{P}_s = \frac{1}{2V} (\sum_i Z_i \Delta_i),$$

where V is the unit-cell volume, Z_i are the effective charges, and Δ_i the atomic displacement vectors required to reverse \mathbf{P}_s . The presence of covalent P-P and P-S bonds in CuInP_2S_6 precludes assumption of point charges in the calculation. The ethanelike P_2S_6 entity may however be treated as a rigid ion. This has been demonstrated in the case of $\text{Sn}_2\text{P}_2\text{S}_6$ where the lattice dynamics could be satisfactorily modeled with a short-range potential dominated by Sn-S interactions and the P_2S_6 taken as an undeformable vibrational unit.²² The model parameters therein were varied to best fit experimental Raman frequencies and gave effective charges of $\text{Sn}^{1.2+}$, $\text{P}^{0.6+}$ and $\text{S}^{0.6-}$, i.e., $(\text{P}_2\text{S}_6)^{2.4-}$. Such charges do not directly correspond to the chemical properties of the compound but are more representative of the bonding than the formal valences. Accordingly, a $-2.4e$ charge may be assumed in place of P_2S_6 in CuInP_2S_6 . Electrical neutrality and proportionality to the chemical valences would then require effective cationic charges of $\text{Cu}^{0.6+}$ and $\text{In}^{1.8+}$.

In the $T < 315$ K CuInP_2S_6 structures, reversal may be effected via a twofold rotation about an axis in the layer midplane, parallel to b and running through the centers of the S_6 octahedral.⁶ This is done most simply by first translating the origin of the monoclinic coordinate system of the structural refinements¹⁸ such that this rotation axis, rather than the indium cation, is located at $z = 0.25$. With (x, y, z) denoting the atomic positions in the translated coordinate system, the positions in the $-\mathbf{P}_s$ structure would be $(-x, y, -z + 1/2)$. Since $\Delta_i = (2x, 0, 2z - 1/2)$, the polarization generally lies

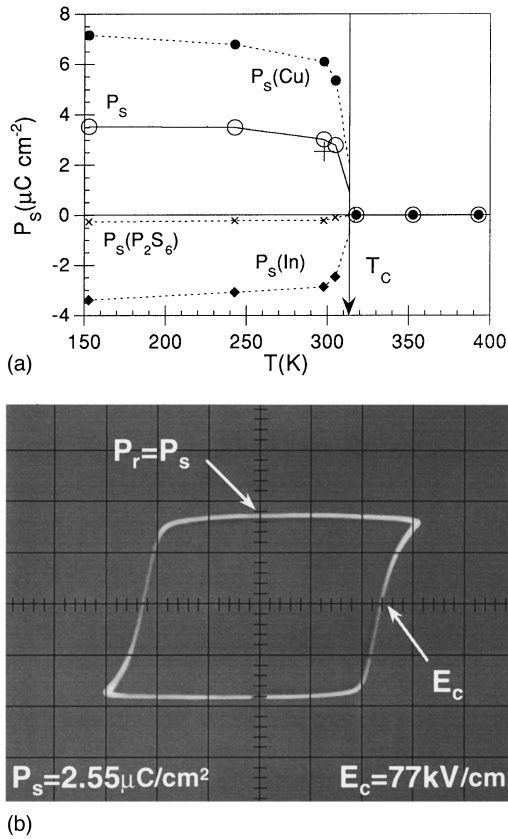


FIG. 4. (a) Polarization P_s and sublattice contributions $P_s(\text{Cu}^I)$, $P_s(\text{In}^{\text{III}})$, and $P_s(\text{P}_2\text{S}_6)$ calculated from crystallographic results on CuInP_2S_6 at various T ; + marks the measured RT value. (b) Saturated RT hysteresis loop for CuInP_2S_6 and the measured P_s and E_c values; a 100 kV cm^{-1} electric field at 50 Hz was applied perpendicular to the layers of a platelike crystal sample.

within the a - c plane. Within experimental error, \mathbf{P}_s is found to be perpendicular to the layer (pseudopolar c^* axis) and is more conveniently described within a Cartesian coordinate system [via the transformations $\mathbf{a} = a\mathbf{i}$ and $\mathbf{c} = c(\cos\beta\mathbf{i} + \sin\beta\mathbf{k})$].

The thermal evolution of P_s ($\mathbf{P}_s \approx P_s \mathbf{k}$) calculated from the crystallographic results is depicted in Fig. 4(a). The contributions from the constituent ions are also shown. Less than 7% of P_s at any temperature could be attributed to the P_2S_6 anions so that the behavior of CuInP_2S_6 should approximate that of a collinear, two sublattice (Cu^I and In^{III}) ferroelectric. These curves are reasonably consistent with a first-order transition occurring around 315 K.¹⁵ Cooling below T_C enhances the polarity of each sublattice down to 153 K; the uncompensated dipole moment however does not appear to grow beyond the value attained at 243 K. A given P_s may conceivably be obtained from different sets of Cu^I and In^{III} contributions, the variation presumably originating in the relative occupancies of the $\text{Cu}1^u$ and $\text{Cu}1^d$ sites. In particular, it is possible that the dipole configuration immediately following (preceding) the loss (appearance) of twofold symmetry is not unique and the resultant P_s close to T_C may have some thermal history dependence. The slight broadening of the ϵ_r' and $\tan \delta$ extrema at the transition and thermally hysteretic shape for the ϵ_r' anomaly noted in earlier dielectric measurements⁵ may be explained by such behavior.

A value of $3.01(4) \mu\text{C cm}^{-2}$ for P_s in CuInP_2S_6 at RT is predicted in Fig. 4(a). This quantity was measured by obtaining a saturated dielectric hysteresis loop using a crystal sample. Figure 4(b) displays the D versus E trace ($\mathbf{D} = \epsilon_0 \mathbf{E} + \mathbf{P}$) which demonstrates the reversibility of the spontaneous polarization and yields $P_s = 2.55 \mu\text{C cm}^{-2}$, fairly close to the calculated value, and 77 kV cm^{-1} for the coercive electric field E_c . The loop is symmetric and rectangular, the remanent polarization practically equaling the spontaneous value and the coercive field being well defined. This suggests an intimate coupling between the Cu^I and In^{III} sublattices which causes them to reorient simultaneously. Also, reverse nucleation apparently does not occur before complete reversal of the applied field. This is probably because domains in this compound would tend to form perpendicular to rather than within the layers, i.e., domain walls appear in the inter-layer space, and the sample used was fairly thin ($\approx 16 \mu\text{m}$). Last, Fig. 4(a) shows that the spontaneous polarization changes very rapidly below T_C , i.e., dP_s/dT may be expected to be quite large in this temperature range. Indeed, initial results of pyroelectric measurements yielded a pyroelectric coefficient of $13 \text{ nC cm}^{-2}/\text{K}$ at 265 K for CuInP_2S_6 .

Other aspects of the CuInP_2S_6 structure that change with the polar character of the cation sublattices are worth considering. Figure 5(a) and 5(b) display the average Cu1-S distance and S-S bond length in the upper and lower triangles of the CuS_6 units as a function of temperature. Cu1-S and S-S values in the centrosymmetric phase are smaller as expected because of the averaging over the upper and lower S_3 triangles which swell (contract) when the associated off-center copper site is filled (empty) as hopping occurs between equivalent Cu1. Upon crossing into the ferroelectric phase, the Cu1-S distance increases and the S-S curve forks following the preponderant filling of the $\text{Cu}1^u$ site. Note that the empty lower S_3 triangle shrinks more than the occupied upper one expands. The asymmetry and distortion of the InS_6 group evolve with temperature in the converse manner as shown in Fig. 5(c) and 5(d). Concomitant changes in the P_2S_6 entity are illustrated in Fig. 5(e). A T -enhanced dispersion of the P-S distances (larger difference between maximum and minimum values) is observed in the paraelectric phase, while length variations associated with the inequivalence of the upper and lower PS_3 appear below T_C . In addition, both PS_3 groups undergo concerted clockwise twists at $T < 315 \text{ K}$ along with counter twists of the InS_6 basal triangles (Fig. 6). No significant T dependence of the P-P distance was detected.

On the basis of the above results, an explanation may be given for the thermal variation of the cell parameters observed in a previous study and partly reproduced in Figs. 7(a) and 7(b). Figure 7(c) plots the layer thickness and width of the interlamellar space, the components of the c parameter, as a function of temperature. Between 153 and 243 K, the layer thickness is constant so that the c parameter increase with warming is due solely to an expansion of the interlamellar gap. At $243 < T < 310 \text{ K}$ the layer becomes thicker presumably as the Cu^I starts to hop between the $\text{Cu}1^u$ and $\text{Cu}1^d$ sites and the probability density around $\text{Cu}1^u$ extends into the gap. The gap expansion is thus enhanced by the partial or occasional filling of the Cu3 site. Upon heating above 315 K,

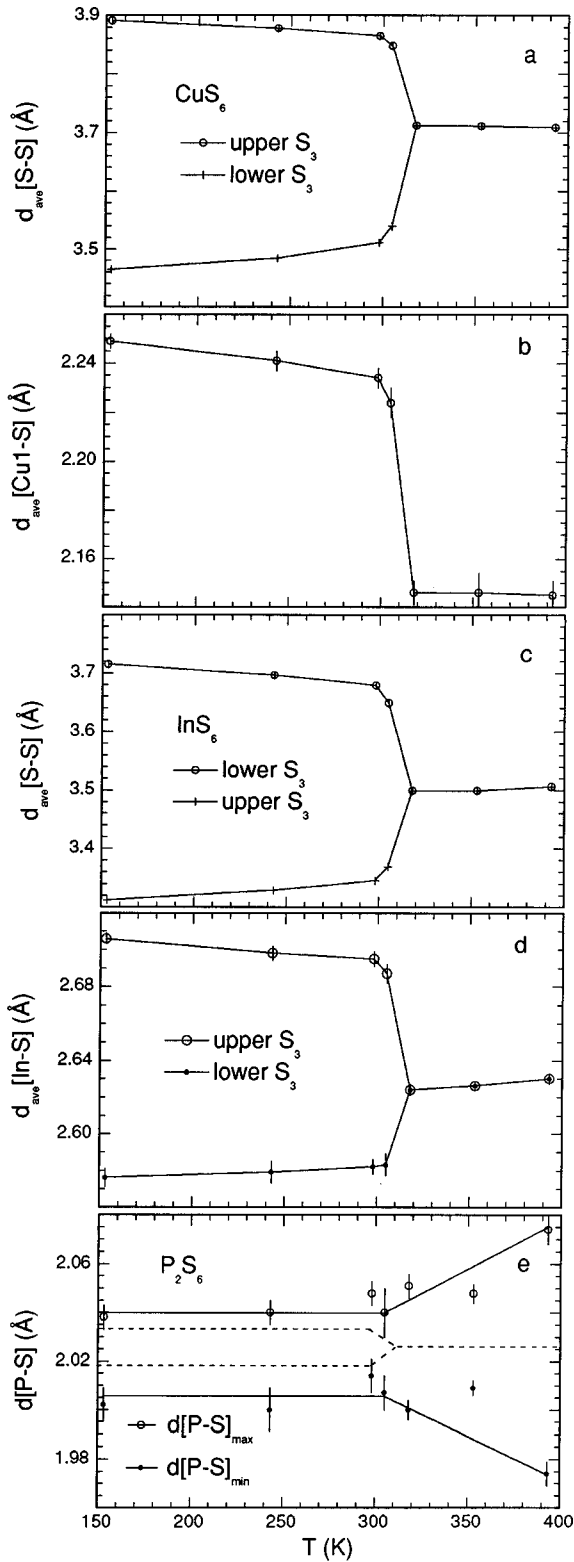


FIG. 5. Thermal variation of (a) the average S-S and (b) Cu1-S distance in a CuS_6 unit; (c) the average S-S and (d) In-S distance in a InS_6 unit; and (e) the maximum and minimum P-S distance within P_2S_6 . The T dependence of the average P-S distance is also shown by the dashed curve in (e). Forked curves illustrate the inequivalence of upper and lower basal triangles of all units below T_C .

the appearance of the twofold axis does not incur sudden change. However, as the symmetric intracage hopping motions and Cu^I excursions into the interlamellar space become more frequent, both the gap width and the layer thickness

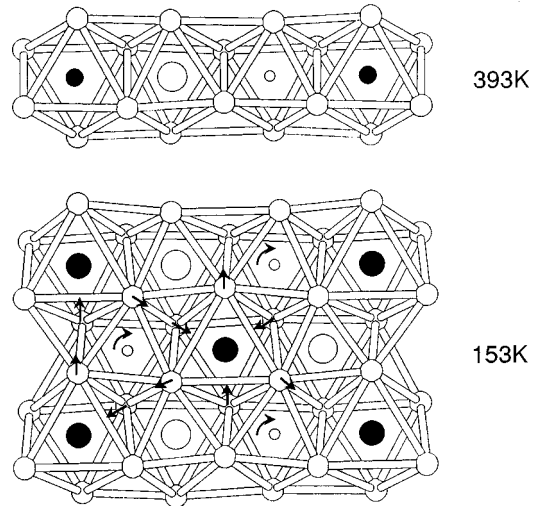


FIG. 6. A layer of CuInP_2S_6 at 153 K showing opposed twists of P_2S_6 and InS_6 basal triangles; the relative orientations of these groups at 393 K are shown as a reference.

increase in the $315 < T < 353$ K range. Between 353 and 393 K, the thickness exhibits no change so the c -parameter thermal variation there once again reflects only the gap expansion.

The a and b parameters undergo normal increases with temperature in the $153 < T < 253$ K and $T > 353$ K regimes. As T_C is approached from below, both a and b increase following changes in the basal CuS_6 and InS_6 triangles, particularly the release of strains in the lower S_3 group of the copper octahedron. The sulfur framework also relaxes and the b parameter lengthens slightly as the twists of the PS_3 and InS_6 basal triangles decrease with heating. In addition, Cu^I hopping motions have nonzero components along the a axis and probably contribute to the a parameter increase with heating. The larger dispersion of the P-S bond lengths in the $315 < T < 353$ K range may also lead to an increase in b .

IV. DISCUSSION

The present study gives a fairly detailed description of how the ferroelectric-paraelectric transition in CuInP_2S_6 transpires, verifying thus the key role played by the Cu^I ion and the principally order-disorder character of the phase transformation. The loss of twofold symmetry with cooling below T_C is shown to be a single-step event, consistent with the expectation of a first-order transition.¹⁵ Information about the dynamics of this system may be gleaned from the static picture given by diffraction. Aside from furnishing indirect evidence for T -dependent copper hopping motions, the crystallographic results indicate how these might couple with the indium displacement and (P_2S_6) deformations. The nature of such processes in the polar, critical, and nonpolar regimes is the subject of our ongoing neutron scattering, vibrational spectroscopy, and NMR experiments. Additional measurements of some thermodynamic properties (e.g., dielectric, pyroelectric) are also being carried out. Of particular interest would be an experimentally determined $P_s = P_s(T)$ curve which may be compared with Fig. 4(a) and should make it

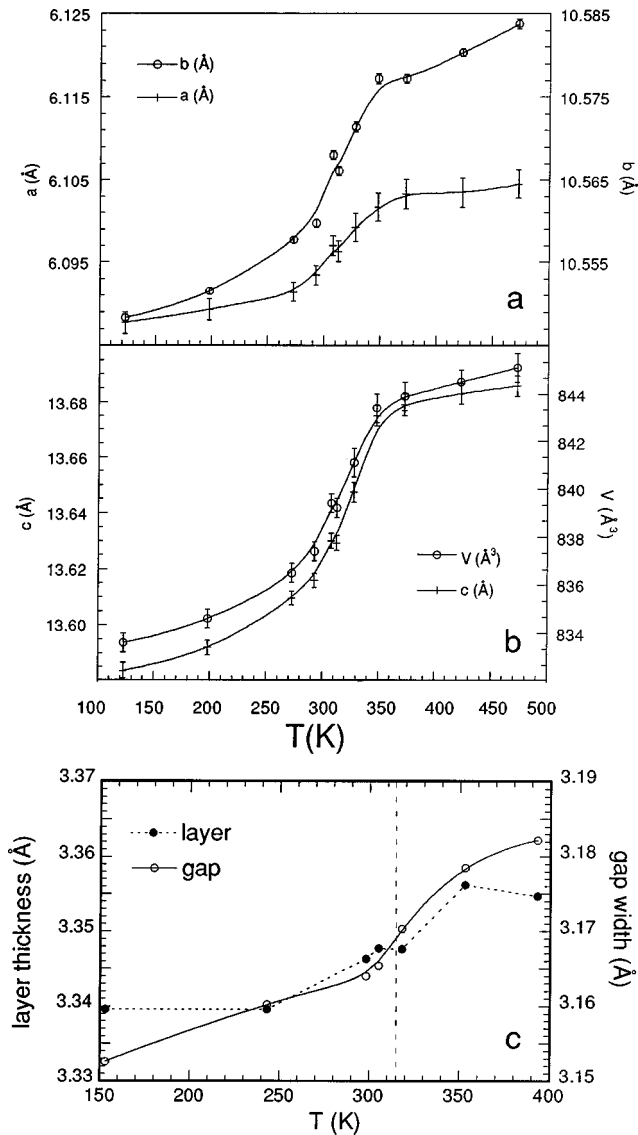


FIG. 7. (a) and (b): Cell parameters a , b , c and the volume V as a function of temperature (Ref. 15). A weak T dependence was found for the angle β [107.13(2), 107.09(2), and 107.12(3) $^\circ$ for $T = 153$, 305, and 393 K, respectively] (Ref. 18). (c) Thermal variation of the layer thickness and interlayer gap width.

possible to describe a Landau type model for the transition to the ferrielectric phase.

Strictly speaking, CuInP_2S_6 at $T < T_C$ does not have a polar symmetry axis (class m) and the atomic shifts required to reverse the polarization occur in the a - c plane. The electric dipole moments associated with the off-centered cations however align with the normal to the layer (c^*), yielding a uniaxial configuration. The saturated P_s calculated for CuInP_2S_6 ($\approx 3.5 \mu\text{C cm}^{-2}$ at 153 K) is smaller than those found in the uniaxial oxygen-octahedra ferroelectrics (11–71 $\mu\text{C cm}^{-2}$).²³ This is of course because the dipoles all have the same sense in the latter while CuInP_2S_6 contains two sets of oppositely directed electric dipoles. On the other hand, P_s in CuInP_2S_6 is larger than those in materials that have traditionally been referred to as ferrielectrics, notably ammonium sulfate²⁴ which has a compensation temperature. Collinear ferrielectric cation sublattices yielding a relatively large polarization ($> 0.1 \mu\text{C cm}^{-2}$) are indeed rather rare.

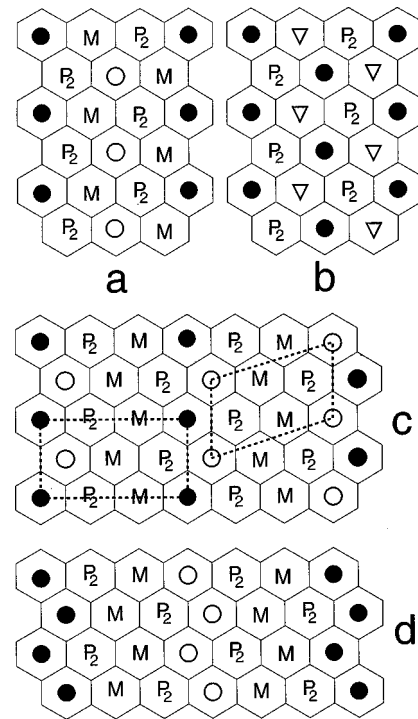


FIG. 8. Possible ferrielectric patterns within a $A^I M^III P_2 S_6$ layer. Up (down) shifted d^{10} ions are represented by black (white) symbols. In a and b , basic triangular (A , M' , P-P) networks are assumed. (a) A “striped” phase with only one d^{10} ion. (b) Phase with d^{10} A (circle) and M (triangle) ions conserving the triangular motif: this is also possible in MPS_3 for a $d^{10} M^{II}$ ion. In (c) and (d) A, M, and P-P form zigzag chains. (c) Phase with antiferroelectric intrachain interactions: two possible interchain couplings are shown. (d) Phase with (anti)ferroelectric (inter)intra-chain interactions.

We have found one other example, that of the rare-earth manganites¹ RMnO_3 ($R = \text{Y, Yb, Er, Ho, Tm, Lu}$) which have a likewise planar array of opposite and unequal R^{III} dipoles and a P_s of about $2.5 \mu\text{C cm}^{-2}$.

Some generalities regarding the origin of the ferrielectric structure of CuInP_2S_6 merit closer examination. As mentioned earlier, the Cu^I preference for quasitrigonal over octahedral coordination in this compound may be ascribed to a second-order Jahn-Teller effect:^{10–12} the off-centering normal to the layer may be viewed as a distortion allowing a mixing of the $3d^{10}$ manifold and $4s$ orbital which are separated by a mere $\approx 2.7 \text{ eV}$.²⁵ The causal relation between $4s/3d$ coupling and an off-center Cu^I displacement has been established theoretically for the zinc-blende semiconductor CuCl for which a symmetry lowering transition was predicted.¹² We are currently performing electronic band-structure calculations to confirm this hypothesis for CuInP_2S_6 . Electric dipole ordering due to a pseudo Jahn-Teller coupling of nearly degenerate electronic levels has long been known to occur in zircons²⁶ of the Kramers ion Dy^{III} . That a similar mechanism causes ferroelectricity in BaTiO_3 is in fact a decades-old suggestion²⁷ which has effectively been borne out by the demonstrated importance of Ti $3d$ and O $2p$ hybridization therein.³ Other octahedrally coordinated d^0 transition metal ions may also undergo out-of-center distortions attributable to a second-order Jahn-Teller coupling. It has, however, been shown via an investi-

gation of a variety of oxide structures that these distortions are not purely electronically driven but derive from a combination of electronic, structural, and Coulomb effects.²⁸ Quite generally then, it may be said that closed-shell cations (d^0 and d^{10}) may off-center because of a second-order Jahn-Teller instability; whether or not ferroelectric order ensues may depend on the detailed characteristics of the host structure.

It is clear from the example of CuInP_2S_6 that electric dipole moments may be associated with d^{10} cations trapped in a high coordination environment created by the anion interstices of a solid. The dipole strength would depend on the extent of the second-order Jahn-Teller instability, i.e., decrease with increasing interconfigurational energy difference,²⁵ as illustrated by the Cu^I and In^{III} moments in CuInP_2S_6 . Cooperative behavior may be envisioned in terms of dipole-dipole correlations developing with a freezing of random d^{10} cation motions, or ordering of their random positions. If the dipoles are part of and orthogonal to a plane or chain, the appearance of long-range order would involve antiparallel displacements which minimize the electrostatic and elastic energy costs of ordering, as demonstrated by the low temperature CuMP_2S_6 ($M = \text{Cr}, \text{In}$) phases.

Two-dimensional ferrielectric geometries are inherent in all the d^{10} -cation-bearing $M^{II}\text{PS}_3$ and $A^I M^{III}\text{P}_2\text{S}_6$ compounds.^{6,8,10,29,30} We note that the presence of flexible polyhedral entities like P_2S_6 appears to favor off centering. Figure 8(a) and 8(b) display the dipole arrangements found in CuCrP_2S_6 at $T < 150$ K and CuInP_2S_6 at $T < 315$ K. The first has only A^I moments (non- d^{10} M^{III}) and assumes a striped appearance; the second retains the triangular motif

via an antidisplacement of the A^I and M^{III} ions, both assumed to be d^{10} . A compensated version of this latter configuration exists in $\text{Hg}_2\text{P}_2\text{S}_6$ and $\text{Hg}_2\text{P}_2\text{Se}_6$ at RT (Ref. 28) along with an approximately tetrahedral Hg^{II} ($5d^{10}$) coordination. More recently, the Cd^{II} ($4d^{10}$) in $\text{Cd}_2\text{P}_2\text{S}_6$ were found to order at $T < 228$ K in a similar antipolar manner.³⁰ For Ag^I ($4d^{10}$) and $M = \text{V}$ or Cr , we know that the cations are disposed in zigzag patterns.¹⁰ Figure 8(c) and 8(d) illustrate the possibilities for this geometry with Ag^I moving off center. It would be interesting to determine if the inter-zigzag distances in these compounds are too large to authorize long-range ordering and lead to "glassy" dipole states instead.

The recipe suggestions of Fig. 8 may be expanded into a broader strategy to access new ferroelectric, dipole glass, and antiferroelectric phases. An obvious first step would be to construct layer or chain structures by surrounding Cu^I with ethanelike (e.g., Si_2Cl_6) or tetrahedral (e.g., PS_4) entities, or reinvestigate already known compounds with such structural characteristics. The example of the natural mineral chalcocite³¹ (Cu_2S), which is ferroelectric, however demonstrates that a polyhedral building block is not essential to dipole ordering. Nevertheless, it appears that incorporating d^{10} cations into systems with anionic polyhedra and anisotropic morphologies would lead to a variety of cooperative dipole phenomena owing to energetically favored ferrielectric configurations therein.

ACKNOWLEDGMENT

The authors would like to thank C. Payen for valuable discussions and his contribution towards the acquisition of the low temperature device for the diffractometer.

*Author to whom correspondence should be sent. Electronic address: cajipe@cnsr-inm.fr

¹ *Ferroelectrics and Related Substances: Oxides/Oxide*, edited by K.-H. Hellwege and O. Madelung, Landolt-Börnstein, New Series, Group III, Vol. 28, Pt. a (Springer-Verlag, Berlin 1989); also, *Ferroelectrics and Related Substances. Non-oxides*, edited by K.-H. Hellwege and O. Madelung, Landolt-Börnstein, New Series, Group III, Vol. 16, Pt. b (Springer-Verlag, Berlin, 1982).

² W. Zhong, D. Vanderbilt, and K. M. Rabe, *Phys. Rev. Lett.* **73**, 1861 (1994).

³ R. E. Cohen, *Nature (London)* **358**, 136 (1992).

⁴ V. Maisonneuve, V. B. Cajipe, and C. Payen, *Chem. Mater.* **5**, 758 (1993).

⁵ V. Maisonneuve, M. Evain, C. Payen, V. B. Cajipe, and P. Molinié, *J. Alloys Compd.* **218**, 157 (1995).

⁶ P. Colombet, A. Leblanc, M. Danot, and J. Rouxel, *J. Solid State Chem.* **41**, 174 (1982).

⁷ V. B. Cajipe, J. Ravez, V. Maisonneuve, A. Simon, C. Payen, R. von der Muhll, and J. E. Fischer, *Ferroelectrics* **185**, 135 (1996).

⁸ E. Durand, G. Ouvrard, M. Evain, and R. Brec, *Inorg. Chem.* **29**, 4916 (1990).

⁹ A. F. Wells, *Structural Inorganic Chemistry* (Oxford University Press, Oxford, 1984), p. 1142.

¹⁰ S. Lee, P. Colombet, G. Ouvrard, and R. Brec, *Inorg. Chem.* **27**, 1291 (1988).

¹¹ J. K. Burdett, *Chemical Bonding in Solids* (Oxford University Press, Oxford, 1995), pp. 24 and 246; J. K. Burdett and O. Eisenstein, *Inorg. Chem.* **31**, 1758 (1992).

¹² S. H. Wei, S. B. Zhang, and A. Zunger, *Phys. Rev. Lett.* **70**, 1639 (1993).

¹³ G. Burr, E. Durand, M. Evain, and R. Brec, *J. Solid State Chem.* **103**, 514 (1993).

¹⁴ The term is used in analogy with "ferrimagnetism," a name suggested in L. Néel, *Ann. Phys. (Paris)* **3**, 137 (1948) to describe magnetic behavior similar to that of ferrites which contain two unequal and oppositely directed magnetic sublattices.

¹⁵ A. Simon, J. Ravez, V. Maisonneuve, C. Payen, and V. B. Cajipe, *Chem. Mater.* **6**, 1575 (1994).

¹⁶ C. Kay Fair, MOLEN: Structure Determination Package, Enraf-Nonius, 1982.

¹⁷ U. H. Zucker, E. Perenthaler, W. F. Kuhs, R. Bachmann and H. Schulz, *J. Appl. Crystallogr.* **16**, 358 (1983); R. Bachmann and H. Schulz, *Acta Crystallogr. Sect. A* **40**, 668 (1984).

¹⁸ See AIP Document No. PAPS PRBMD-56-10 860-5 for 5 pages of supplementary material (recording and refinement conditions, cell parameters, atomic positions, and thermal factors). Order by PAPS number and journal reference, from American Institute of Physics, Physics Auxiliary Publication Service, Carolyn Gehlbach, 500 Sunnyside Boulevard, Woodbury, New York 11797-2999. Fax: 516-576-2223, e-mail: paps@aip.org. The price is \$1.50 for each microfiche (98 pages) or \$5.00 for photocopies of up to 30 pages, and \$0.15 for each additional page over 30 pages. Airmail additional. Make checks payable to the American Institute of Physics.

¹⁹ W. F. Kuhs, *Acta Crystallogr. Sect. A* **48**, 80 (1992). **39**, 148 (1983).

- ²⁰V. Maisonneuve, J. M. Réau, M. Dong, V. B. Cajipe, C. Payen, and J. Ravez, *Ferroelectrics* **196**, 257 (1997).
- ²¹W. C. Hamilton, *Acta Crystallogr.* **18**, 502 (1965).
- ²²A. A. Grabar, Yu. M. Vysochanskii and V. Yu. Slivka, *Fiz. Tverd. Tela (Leningrad)* **26**, 3086 (1984) [*Sov. Phys. Solid State* **26**, 1859 (1984)].
- ²³S. C. Abrahams and E. T. Keve, *Ferroelectrics* **2**, 129 (1971).
- ²⁴A. Onodera, O. Cynshi, and Y. Shiozaki, *J. Phys. C* **18**, 2831 (1985), and references therein.
- ²⁵C. E. Moore, in *Atomic Energy Levels*, Natl. Bur. Stand. (U.S.), Natl. Stand. Ref. Data Ser. No. 35 (U.S. GPO, Washington, DC, 1970). $E(nd^{10}) - E(nd^9[n+1]s^1)$ values for Cu^I , Ag^I , Hg^{II} , Zn^{II} , Cd^{II} , and In^{III} are 2.7, 4.9, 5.3, 9.7, 10.0, and 16.0 eV, respectively.
- ²⁶G. A. Gehring and K. A. Gehring, *Rep. Prog. Phys.* **38**, 1 (1975); D. R. Taylor, S. R. P. Smith, and J. H. Page, *J. Phys. C* **18**, 3285 (1985).
- ²⁷R. Englman, *The Jahn-Teller Effect in Molecules and Crystals* (Wiley, London, 1972), p. 170.
- ²⁸M. Kunz and I. D. Brown, *J. Solid State Chem.* **115**, 395 (1995).
- ²⁹M. Z. Jandali, G. Eulenberger, and H. Hahn, *Z. Anorg. Allg. Chem.* **447**, 105 (1978).
- ³⁰F. Boucher, M. Evain, and R. Brec, *J. Alloys Compd.* **215**, 63 (1994); F. Boucher, M. Evain, and R. Brec, *Acta Crystallogr. Sect. B* **51**, 952 (1995).
- ³¹M. Z. Bienuolis, C. E. Corry, and E. R. Hoskins, *Geophys. Res. Lett.* **14**, 135 (1987).